frontiers | Frontiers in Soft Matter

TYPE Original Research
PUBLISHED 19 July 2022
DOI 10.3389/frsfm.2022.959542

OPEN ACCESS

EDITED BY
Tommy Nylander,
Lund University, Sweden

REVIEWED BY
Yuri Gerelli,
Marche Polytechnic University, Italy
Fabrice Cousin,
UMR12 Laboratoire Léon Brillouin (LLB), France

*CORRESPONDENCE
Masaki Nakahata,
nakahata.masaki.sci@osaka-u.ac.jp
Motomu Tanaka,
tanaka@uni-heidelberg.de

SPECIALTY SECTION
This article was submitted to Self-Assembly and Self-Organisation, a section of the journal Frontiers in Soft Matter

RECEIVED 01 June 2022
ACCEPTED 30 June 2022
PUBLISHED 19 July 2022

CITATION
Yamamoto A, Hayashi K, Sumiya A, Weissenfeld F, Hinatsu S, Abuillan W, Nakahata M and Tanaka M (2022), Modulation of viscoelasticity and interfacial potential of polyelectrolyte brush by Ion-specific interactions. *Front. Soft. Matter* 2:959542. doi: 10.3389/frsfm.2022.959542

Modulation of viscoelasticity and interfacial potential of polyelectrolyte brush by Ion-specific interactions

Akihisa Yamamoto[1], Kentaro Hayashi[1], Ai Sumiya[2], Felix Weissenfeld[3], Satoko Hinatsu[1], Wasim Abuillan[3], Masaki Nakahata[2,4]* and Motomu Tanaka[1,3]*

[1]Center for Integrative Medicine and Physics, Institute for Advanced Study, Kyoto University, Kyoto, Japan, [2]Department of Materials Engineering Science, Graduate School of Engineering Science, Osaka University, Osaka, Japan, [3]Physical Chemistry of Biosystems, Institute of Physical Chemistry, Heidelberg University, Heidelberg, Germany, [4]Department of Macromolecular Science, Graduate School of Science, Osaka University, Osaka, Japan

Polyelectrolyte brushes have drawn increasing attention because their physicochemical properties can be modulated by adjustment of the pH and ion concentration. Here, we report the controlled grafting of poly acrylic acid containing cysteine side chains onto supported lipid membranes to allow for the modulation of viscoelasticity as well as interfacial potential by ion-specific interactions, that is, with cadmium ions. Quartz crystal microbalance with dissipation indicated that the resonance frequency increased and the dissipation decreased as the cadmium concentration increased, attributed to the dehydration of brushes. Systematic variation of the molecular structure demonstrated that the coexistence of thiol and carboxyl moieties is necessary for the viscoelastic response, suggesting that these structural features, common with naturally occurring proteins, form complexes with cadmium ions. Analysis of the height fluctuation of colloidal particles by reflection interference contrast microscopy indicated that the change in the viscoelasticity of the polymer brush layer alters the curvature of the effective interfacial potential. Intriguingly, we found that modulation of the viscoelasticity and interfacial potential caused by calcium ions is weak, suggesting that the interaction is ion-specific. Polymer brushes that can alter the interfacial potential through changes in the degree of hydration opens new avenues for the design of smart, adaptable surfaces.

KEYWORDS

polyelectrolyte brush, ion specificity, interface viscoelasticity, quartz crystal microbalance, microinterferometry, interfacial potential

1 Introduction

Biological systems generally adjust their surfaces flexibly in response to environmental changes under the action of homeostasis. During the past several decades, inspired by nature, advances have been made to develop materials that adapt their physical characteristics in response to external stimuli. In particular, stimulus-responsive polymers have drawn increasing attention for various applications, ranging from coating to drug delivery and tissue engineering (Stuart et al., 2010).

Among polymer materials, polyelectrolyte brushes have been used to fabricate materials with smart, adaptable surfaces, specifically their surface physical properties, such as surface charge density, film thickness, viscoelasticity, and surface friction, can be modulated by subtle changes in the pH and salt concentration (Rühe et al., 2004; Ballauff and Borisov, 2006; Zhou and Huck, 2006; Wu et al., 2007). The interaction between polyelectrolyte brushes and ions, which distinguishes polyelectrolytes from neutral polymers, has been studied intensively, both experimentally and theoretically (Pincus, 1991; Förster and Schmidt, 1995). At low salt concentrations, polyelectrolyte brushes are osmotically swollen, called osmotic brushes. Under this condition, the brush thickness H is independent of the grafting density, and the physical properties of the brush, such as chain conformation, are dominated by electrostatic interactions because the Debye screening length κ^{-1} is larger than the thickness, that is, $\kappa^{-1} > H$. In contrast, at high salt concentrations, the brush thickness H decreases with increasing salt concentration C_s, that is, $H \propto C_s^{-\frac{1}{3}}$ (Borisov et al., 1994; Zhulina et al., 1995; Ahrens et al., 1998). Ahrens et al. deposited a monolayer of poly (ethyl ethylene)-*block*-poly (styrene sulfonate) at the air/water interface and performed specular X-ray reflectivity experiments at a defined area per molecule and surface pressure, thus demonstrating that osmotic brushes transform into salted brushes under systematic variation of C_s (Ahrens et al., 1998). Wu et al. systematically investigated the influence of pH, salt concentration, and grafting density on the thickness of poly (acrylic acid) brushes using spectroscopic ellipsometry at various pH and salt concentrations ranging from 10^{-6}–10^{0} M (Wu et al., 2007).

The degree of ionization of strongly dissociated (quenched) polyelectrolyte brushes is independent of pH, while the degree of ionization of weakly dissociated (annealed) polyelectrolyte brushes is significantly altered by the pH. Thus, effective design strategies for switchable and adaptable surfaces include grafting weakly dissociated polyelectrolyte brushes and adjusting the pH at high salt concentrations, typically $C_s > 100$ mM corresponding to $\kappa^{-1} < 1$ nm (Israelachvili, 1985). Previously, we prepared a monolayer of a diblock copolymer based on a hydrophobic poly (methyl methacrylate) and a weak polyelectrolyte poly [2-(dimethylamino)ethyl methacrylate] at the air/water interface. We then compressed the film to a defined surface area and pressure and deposited the film on solid substrates (Rehfeldt et al., 2006a; Rehfeldt et al., 2006b). The monolayer was transferred from the air/water interface to a hydrophobic substrate using the Langmuir–Schaefer method, which enables precise control of the grafting density (Langmuir and Schaefer, 1938) and is thus advantageous over physisorption from solutions or direct grafting of homopolymer brushes onto solid substrates. Specular neutron reflectivity data demonstrated clear switching of the brush thickness and degree of hydration with changes in the pH, between 5.5 and 8.5. Because switching of the brush conformation occurs near pH 7.0 ± 1.5, this surface can be applied to reversibly switch the interaction between lipid membranes and underlying solid substrates (Rehfeldt et al., 2006b).

Polyelectrolyte brushes also undergo drastic swelling and shrinkage in response to specific ions. Biesalski et al. reported that highly swollen, cationic poly (*N*-methylpyridinium) brushes collapse when the iodide ion concentration is elevated to $[I^-] \approx 0.1$ M, although further increases in concentration to $[I^-] > 1$ M result in re-swelling (Biesalski et al., 2004). To date, ion-specific salting-in and salting-out phenomena have been reported not only for cationic polyelectrolyte brushes but also for proteins, amino acids, and charged surfactants in aqueous media containing counter ions at high salt concentrations (Arakawa and Timasheff, 1984; Tomé et al., 2013; Mehringer et al., 2021). In fact, salting-out of cellular proteins by saturated NaCl solutions is a key process in DNA extraction (Miller et al., 1988). Negatively charged, linear biopolymers, such as alginate, tend to form viscoelastic gels in the presence of divalent cations, such as Ca^{2+} ions (Thiele, 1967; Morris et al., 1978; Gouin, 2004). It is well established that crosslinking of lipopolysaccharides with carboxylate and phosphate side chains via Ca^{2+} and Mg^{2+} on the cell surface is critical for the survival of Gram negative bacteria against cationic antibacterial peptides (Beveridge, 1981). Monte Carlo simulation and high-energy specular X-ray reflectivity showed that negatively charged saccharide chains collapse upon binding of divalent cations and create an electrostatic barrier against cationic antibacterial peptides (Pink et al., 2003; Oliveira et al., 2009; Schneck et al., 2009). Interfacial shear rheology demonstrated that a lipopolysaccharide monolayer at the air/water interface becomes predominantly elastic by the addition of Ca^{2+} in the water subphase (Herrmann et al., 2015).

In this study, we grafted poly (acrylic acid) brushes with biotin terminal groups onto planar lipid membranes (supported lipid membranes) doped with biotinylated lipids with the aid of neutravidin crosslinkers (Scheme 1) and investigated how ion-specific interactions modulated the viscoelasticity and effective interfacial potential. To realize specific affinity to Cd^{2+} ions, we added cysteine side chains to X mol% of total monomers, mimicking naturally occurring phytochelatin in plant cells and metallothionein in animal cells, possessing both –COOH and –SH moieties (Hamer, 1986; Cobbett, 2000). Grafting of

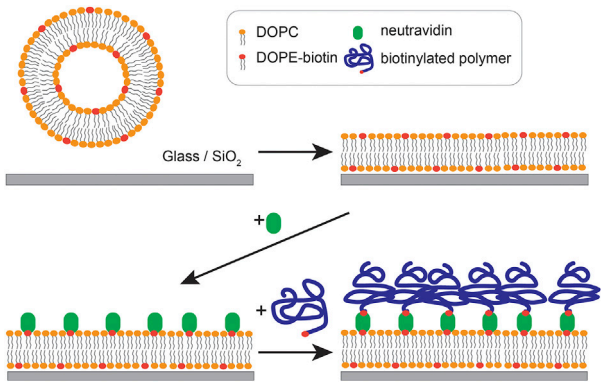

SCHEME 1
Grafting of polymer brushes onto supported membrane surface.

biotin-modified polymers to supported membranes via neutravidin linkers allows for homogeneous grafting of polymers with a well-defined average distance between the polymers $\langle d \rangle$ simply by changing the molar fraction of biotinylated lipids χ_{biotin}, $\langle d \rangle = (A_{\text{lipid}}/\chi_{\text{biotin}})^{0.5}$, where A_{lipid} is the area occupied by one lipid molecule, that is, $A_{\text{lipid}} \approx 0.6\ \text{nm}^2$ (Kaindl et al., 2012; Rieger et al., 2015; Amadei et al., 2018). Modulation of viscoelasticity of the brushes was monitored using quartz crystal microbalance with dissipation (QCM-D) (Moya et al., 2005; Hollingsworth et al., 2019), while changes in the curvature of interfacial interaction potential were determined by analyzing the vertical Brownian motion of latex particles using microinterferometry, called reflection interference contrast microscopy (RICM) (Monzel et al., 2015; Higaki et al., 2017; Amadei et al., 2018).

2 Materials and methods

2.1 Materials

1,2-Dioleoyl-sn-glycero-phospho-ethanolamine-3-*N*-(cap biotinyl) (biotin-DOPE) and 1,2-dioleoyl-sn-glycero-3-phosphocholine (DOPC) were purchased from Avanti Polar Lipids (Alabaster, AL, United States). De-glycosylated neutravidin was purchased from Invitrogen (Tokyo, Japan). Unless stated otherwise, all chemicals, purchased from FUJIFILM Wako Pure Chemical (Osaka, Japan), Nacalai Tesque (Kyoto, Japan), Sigma-Aldrich (St. Louis, MO, United States), or Japan Alcohol Trading (Tokyo Japan), were used without further purification.

The chemical structures of polymers synthesized are shown in Figure 1. pAA-Cys*X*-biotin (*X* = 0, 5, and 20) were synthesized through copolymerization of acrylic acid (AA for pAA) and *S*-trityl-cysteine acrylamide (*S*-Tri-Cys-AAm). Here *X* denotes mol% content of *S*-Tri-Cys-AAm over all monomers. For the synthesis of pPEGMA-Cys5-biotin, acrylic acid was replaced with poly (ethylene glycol) methyl ether acrylate (PEGMA). 4,4'-((*E*)-diazene-1,2-diyl)bis (4-cyano-*N*-(2-(5-((3a*R*,4*R*,6a*S*)-2-oxohexahydro-1*H*-thieno [3,4-*d*]imidazol-4-yl)pentanamido) ethyl)pentanamide) (ACVA-biotin) and 2-(dodecylthiocarbonothioylthio)-2-methylpropionic acid (DDMAT) were used as the initiator and chain transfer agent, respectively. After the copolymerization, the trityl group was deprotected with trifluoroacetic acid (TFA). See Supplementary Material S1 for details of the synthesis and basic characterization of the polymers.

For QCM-D experiments, AT cut quartz crystals (5 MHz) coated with SiO_2 (QSX 303, QSense, Gothenburg, Sweden) were soaked in 2 wt% sodium dodecyl sulfate (SDS) solution for 1 h, followed by rinsing with ultrapure water, drying under a N_2 stream, and treatment in a UV-ozone cleaner for 20 min (Makky and Tanaka, 2015). For RICM experiments, the glass substrates (Menzel, Braunschweig, Germany) were cleaned using a modified RCA method (Kern and Puotinen, 1970), intensively rinsed with water, dried at 70 °C, and stored in a vacuum chamber. The cleaned substrates were bonded to a bottomless plastic round dish from Matsunami Glass (Osaka, Japan). A $CHCl_3$ solution of DOPC doped with DOPE-biotin ($\chi_{\text{biotin}} = 0.02$) was exposed to a nitrogen stream and then kept in a vacuum chamber at 25°C overnight. After suspending the dry lipid films in 100 mM NaCl aqueous solution buffered with 10 mM Tris-HCl (pH = 7.4), the suspension was sonicated with a tip sonicator (Misonix, New York, United States) for 30 min at 1.0 W, yielding small unilamellar vesicles (SUVs). To prepare supported membranes, SUV suspensions were deposited on cleaned glass substrates, and the remaining vesicles were washed off by intensive rinsing. The supported membrane was incubated in neutravidin solution (5 μg/ml) for 1 h, followed by intensive rinsing. Finally, the sample was incubated with an aqueous solution of the biotinylated polymer (0.1 mg/ml) overnight, and the unbound polymers were washed off.

2.2 Methods

2.2.1 Quartz crystal microbalance with dissipation (QCM-D)

Quartz crystal microbalance with dissipation (QCM-D) was used to detect changes in the resonance frequency shift (Δf) and energy dissipation shift (ΔD) caused by deposition of the membranes, coupling of neutravidin and polymers, and interaction of brushes with ions. QCM-D data were recorded using a Q-Sense E4 (Gothenburg, Sweden). QCM-D crystals were cleaned in 10 mM sodium dodecyl sulfate (SDS), rinsed in water, and kept in a UV-ozone chamber for 20 min before each measurement. All measurements were recorded at every odd

overtone up to the 13th overtone throughout the study. For the analysis, we have used the data from fifth, seventh and ninth overtones. In this paper, all data were normalized to the fundamental frequency (5 MHz) by dividing the result with overtone number 5.

2.2.2 Reflection interference contrast microscopy (RICM)

Before starting the observation, latex particles of 10 μm in diameter and 1.04 g/cm^3 in density (Polysciences, Warrington, PA, United States) were passivated by incubating with bovine serum albumin (BSA) solution (1 mg/ml) for 15 min. Although it is still possible that charged patches of BSA may interact with anionic polymers (Seyrek et al., 2003), we found particles showed no clear sign of pinning. All fluctuation experiments were carried out at 298 K using an Axio Observer Z1 microscope (Zeiss, Oberkochen, Germany) equipped with an oil-immersion objective lens (NA 1.25, 63 ×, PH3). Monochromatic light from a high-pressure metal halide lamp (λ = 546 nm) was selected using a band-pass filter. Two polarizers were inserted into the light path in an orthogonal manner: one in the illumination path and the other in the detection path. A λ/4-plate was inserted behind the front lens of the objective, and the illumination numerical aperture (INA) was adjusted to 0.48. 1,000 consecutive images were acquired using an Orca-Flash4.0 camera (Hamamatsu Photonics, Hamamatsu, Japan) at an exposure time of 30 ms for analysis.

First, the lateral drift was corrected using an edge detection filter for each image. Each interference pattern was radially integrated, and two consecutive maximum and minimum nearest to the center were selected. The simplified theory for a normal incident light was applied to perform the conversion of intensity I_{xy} relative to height Δh_{xy} for all pixel positions between the maximum and minimum[24]:

$$\frac{2I_{xy} - (I_{\max} + I_{\min})}{I_{\max} - I_{\min}} = \cos\left[\frac{4\pi n_{\text{med}} \Delta h_{\text{xy}}}{\lambda}\right] \tag{1}$$

Δh_{xy} was calculated for all frames and used to obtain the relative bead position $\Delta h = \Delta h_{xy} - \langle \Delta h_{xy} \rangle$. All analyses were performed using a self-written routine in Matlab (R2014b) (Higaki et al., 2017).

2.3 RICM data analysis

The vertical Brownian motion of a particle in the interfacial potential $V(\Delta h)$ is given by a Langevin equation:

$$m\frac{\partial^2 \Delta h}{\partial t^2} + \gamma \frac{\partial \Delta h}{\partial t} + \frac{\partial V}{\partial \Delta h} = F_{\text{stoch}}. \tag{2}$$

Here, m is the mass of a particle, γ is the friction coefficient, Δh is the relative height of the particle position, and F_{stoch} is the stochastic force. The first acceleration term is negligible because particle movement is overdamped (Pincus, 1991). The second term is the frictional force given by the Reynolds equation (Reynolds, 1883):

$$\gamma = \frac{6\pi \eta_{\text{eff}} R^2}{h}. \tag{3}$$

Here, η_{eff} is the effective viscosity and $\frac{\partial \Delta h}{\partial t}$ is the relative velocity. If one assumes $\frac{\partial \Delta h}{\partial t} \approx 10\,\text{nm}/0.03\,\text{s} = 3\times10^{-7}\,\text{m/s}$, the Reynolds number Re of the system estimated from the density of the latex particle ρ = 1.04 g/cm^3, particle radius $R \approx 5$ μm, and viscosity of water $\eta_{\text{eff}} = 1\,\text{m}\,\text{Nm}^{-2}\text{s}$ is

$$Re \leq R\left(\frac{\partial \Delta h}{\partial t}\right)\rho \eta_{\text{eff}} \sim 10^{-4}, \tag{4}$$

which is far below 1. Note that the effective interfacial potential near the minimum can be approximated as a harmonic (Derjaguin, 1987): $V(\Delta h) = \frac{1}{2}V''\Delta h^2$. The autocorrelation function of height fluctuation can be calculated within the framework of the fluctuation–dissipation theorem:

$$\langle \Delta h(\delta t)\Delta h(0)\rangle \approx \langle \Delta h^2(0)\rangle e^{-\frac{\delta t}{\tau}}. \tag{5}$$

The mean squared amplitude of the fluctuation $\Delta h^2(0) = k_B T/V''$ is given by the equipartition theorem and $\tau = \gamma/V''$. Under thermodynamic equilibrium, the effective interfacial potential $V(\Delta h)$ can also be calculated from the probability function of the fluctuation amplitude $P(\Delta h)$, following the inverse work functional theorem (Albersdörfer and Sackmann, 1999; Monzel et al., 2015; Higaki et al., 2017):

$$V(\Delta h) = -k_B T \ln P(\Delta h) + \text{const.} \tag{6}$$

3 Results and discussion

3.1 Grafting of polymer brushes onto supported membranes

As shown in Scheme 1, the membrane was first incubated with a neutravidin solution prior to the grafting of polymer brushes. Figure 2A shows the change in Δf and ΔD caused by successive deposition of (I) a supported lipid membrane (II) neutravidin crosslinkers, and (III) pAA-Cys5-biotin (Figure 1A, X = 5). Following the establishment of a baseline in the buffer, the sample was incubated with a suspension of DOPC vesicles doped with 2 mol% DOPE, corresponding to $\langle d \rangle$ = 5.5 nm. The obtained shift in frequency and dissipation after vesicle fusion and neutravidin binding are in good agreement with the previous reports, confirming the deposition of a planar lipid membrane and the binding of neutravidin (Keller et al., 2000; Körner et al., 2013; Amadei et al., 2018). The layer parameters obtained by the fitting of QCM-D response using Voigt-Voinova model (Vogt

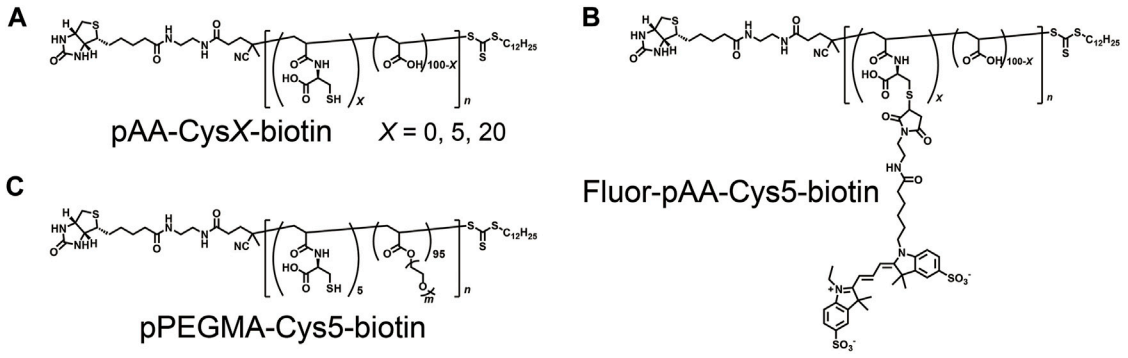

FIGURE 1
Chemical structures of polymers used in this study. **(A)** pAA-CysX-biotin (*X* = 0, 5, 20), **(B)** Fluor-pAA-Cys5-biotin, and **(C)** pPEGMA-Cys-biotin. *X* denotes mol% content of *S*-Tri-Cys-AAm over all monomers.

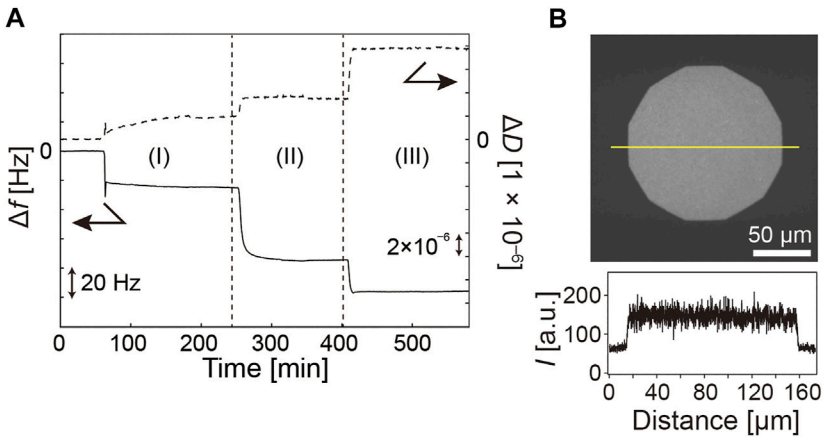

FIGURE 2
Characterization of pAA-Cys5 brushes on supported membrane surface. **(A)** Formation of a supported membrane (I), coupling of neutravidin crosslinker (II), and coupling of pAA-Cys5-biotin (III), monitored by QCM-D. Each step could be detected as changes in the resonance frequency Δf and dissipation ΔD. **(B)** Fluorescence microscopy image of Fluor-pAA-Cys5-biotin grafted onto a supported membrane. Average distance between polymers is $\langle d \rangle$ = 5.5 nm. The line profile confirms the uniform coating of the membrane surface with polymer brushes.

et al., 2004) were presented in Supplementary Material Table S2. After the incubation with pAA-Cys5-biotin solution and the successive rinsing (III), we observed a further decrease in Δf and an increase in ΔD by the grafting of polymer brushes, $\Delta f \approx -21$ Hz and $\Delta D \approx 4.1 \times 10^{-6}$. The brush layer thickness, shear elasticity and viscosity calculated with the same model are $d_{\text{pAA-Cys5}} \approx 13$ nm, $\mu \approx 13 \times 10^3$ Pa, and $\eta = 1.0 \times 10^{-3}$ Pa·s, respectively. Homogeneous grafting of polymer brushes onto a supported membrane was also confirmed by grafting a fluorescently labeled polymer, Fluor-pAA-Cys5-biotin (Figure 1B). Figure 2B shows the fluorescence microscopy image of a supported membrane functionalized with Fluor-pAA-Cys5-biotin. The fluorescence signal was continuous all over the surface, and the constant intensity profile across the whole field of view confirmed that the membrane surface was uniformly coated with polymer brushes.

3.2 Viscoelastic response of pAA-Cys5 brush is reversible and dependent on $[Cd^{2+}]$

Figure 3A shows the change in Δf (solid line) and ΔD (broken line) under a step-wise increase in $[Cd^{2+}]$ over time. In the following, both Δf and ΔD values at $[Cd^{2+}] = 0$ M were set as the reference levels to compare the response of polymer brushes to Cd^{2+} ions. As presented in Figure 3B, Δf monotonically

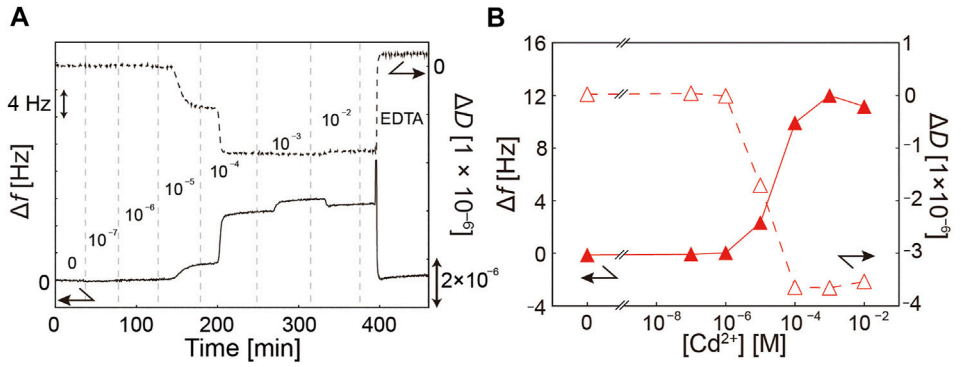

FIGURE 3
Response of pAA-Cys5 to Cd^{2+} ions detected by QCM-D. **(A)** Change in Δf and ΔD under a step-wise variation of $[Cd^{2+}]$ over time. **(B)** Δf and ΔD plotted as a function of $[Cd^{2+}]$. Distinct increase in Δf and decrease in ΔD could be detected at $[Cd^{2+}] \geq 10^{-5}$ M, indicating the loss of water molecules bound to pAA-Cys5 chains. Note that Δf and ΔD came back to the original values after rinsing with the buffer containing 10 mM EDTA and 100 mM NaCl, confirming that the response of pAA-Cys5 to Cd^{2+} can be switched reversibly.

increased and ΔD monotonically decreased with increasing $[Cd^{2+}]$. An increase in Δf and decrease in ΔD was clearly observed at $[Cd^{2+}] \geq 10^{-5}$ M. The increase in Δf suggests that the binding of Cd^{2+} to pAA-Cys5 caused the loss of water molecules associated with the brushes, while the decrease in ΔD suggests that the binding of Cd^{2+} makes the pAA-Cys5 layer becomes less dissipative and hence more elastic. Notably, the fitting results of QCM-D response exhibited large errors at $[Cd^{2+}] \geq 10^{-4}$ M (Supplementary Table S3), implying that Voigt-Voinova model is no longer valid at high $[Cd^{2+}]$ due to the damping of dissipation from $\Delta D \approx 0$ (0 M, reference level) to $\Delta D \approx -3.7 \times 10^{-6}$ (10^{-4} M). Under these conditions, pAA-Cys5 brushes are very poorly hydrated and thus water is no longer a good solvent. We observed a very minor shift in Δf and ΔD values in the opposite direction when $[Cd^{2+}]$ was elevated from 10^{-3} M to 10^{-2} M, suggesting that the response already reached to the saturation level. Note that both Δf and ΔD came back very close to the original values (0 M) once pAA-Cys5 brushes were rinsed with the buffer containing 10 mM EDTA and 100 mM NaCl. As the deviations of both Δf and ΔD are minor (+1.9 Hz and $+0.1 \times 10^{-6}$), we presume that the response of pAA-Cys5 to Cd^{2+} ions is reversible.

3.3 $[Cd^{2+}]$-dependent interaction originates from side-chain functionalities

In the next step, we addressed the following question: what is the structural origin of the prominent $[Cd^{2+}]$-dependent viscoelastic response of pAA-Cys5? Structurally, pAA-Cys5 possesses both –COOH and –SH side chains. It is possible that these two side chains play key roles in the $[Cd^{2+}]$-dependent response because this is a common feature shared with naturally occurring proteins, such as metallothionein and phytochelatin. Additionally, it is well established that cysteine forms solid-state complexes with Zn^{2+} and Cd^{2+} ions (Shindo and Brown, 1965), whereas polysaccharides with –COOH motifs, such as alginate, tend to form egg-box like complexes with Ca^{2+} (Morris et al., 1978).

To unravel how the –SH group affects the interaction with Cd^{2+} ions, we monitored the interaction of pAA-Cys0 (no –SH groups, Figure 1A, $X = 0$) with Cd^{2+} ions. Figure 4A shows the Δf (solid symbols) and ΔD (open symbols) of pAA-Cys0 brushes as a function of $[Cd^{2+}]$. Compared with pAA-Cys5 (Figure 3B), pAA-Cys0 showed a markedly lower response. In particular, Δf increased by + 4.9 Hz and ΔD decreased by -0.5×10^{-6} as $[Cd^{2+}]$ increased from 0 to 10^{-2} M. Moreover, the direction of shift was opposite for both Δf and ΔD, suggesting that increasing $[Cd^{2+}]$ led to a slight increase in the amount of water molecules associated with pAA-Cys0 brushes. The opposite trend in response as well as the lower changes in both Δf and ΔD suggest that the mode of interaction between pAA-Cys0 (–COOH only) and Cd^{2+} ions is distinct from that between pAA-Cys5 (both –COOH and –SH) and Cd^{2+} ions. Next, to study the influence of –COOH groups on the interaction with Cd^{2+} ions, we monitored the interaction of pPEGMA-Cys5 (no –COOH groups, Figure 1C) with Cd^{2+} ions. Figure 4B shows the Δf and ΔD of pPEGMA-Cys5 attached to a supported membrane in the absence and presence of 1 mM Cd^{2+} ions, showing almost no response to Cd^{2+} ions. The obtained data clearly indicate that the co-existence of both –COOH and –SH groups are necessary to respond to Cd^{2+} ions.

We further investigated how the molar fraction of –SH side chains affect the viscoelastic response by grafting pAA-Cys20-biotin (Figure 1A, $X = 20$) onto the supported membrane doped with 2 mol% DOPE-biotin. Figure 4C shows the change in Δf (solid symbols) and ΔD (open symbols) of pAA-Cys20 brushes as a function of $[Cd^{2+}]$. It is notable that pAA-Cys20 exhibited qualitatively the same tendency as pAA-Cys5 (Figure 3B).

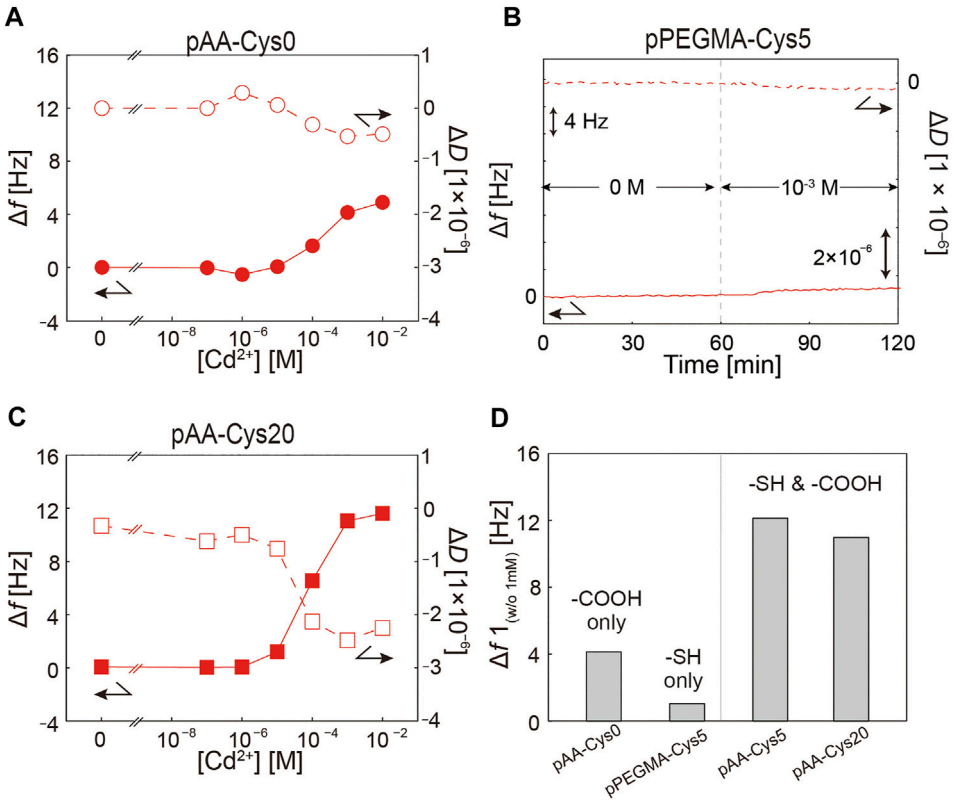

FIGURE 4
Dependence of Δf and ΔD on $[Cd^{2+}]$ for of polymers with different structures. **(A)** pAA-Cys0-biotin, **(B)** pPEGMA-Cys5-biotin, and **(C)** pAA-Cys20-biotin. **(D)** Significance of response to Cd^{2+} ions. For comparison, the difference in Δf between $[Cd^{2+}] = 10^{-3}$ M and 0 M was plotted for each polymer.

Increasing $[Cd^{2+}]$ led to a monotonic increase in Δf and ΔD, and the response became prominent at $[Cd^{2+}] \geq 10^{-5}$ M. It is notable that the change in both Δf and ΔD was lower for pAA-Cys20 than for pAA-Cys5, suggesting that the response did not increase monotonically with increasing molar fraction of the –SH moiety *X*. Figure 4D shows a comparison of the changes in Δf and ΔD between $[Cd^{2+}] = 10^{-3}$ M and 0 M for pAA-Cys0, pAA-Cys5, pAA-Cys20, and pPEGMA-Cys5. Our data demonstrated that the presence of both –COOH and –SH groups is prerequisite for $[Cd^{2+}]$-dependent modulation of the interfacial viscoelasticity, and the sensitivity does not increase with increasing molar fraction of the –SH group. The changes in Δf and ΔD recorded for pAA-Cys0 and pAA-Cys20 are presented in Supplementary Figure S4.

3.4 Modulation of effective interfacial potential $V(\Delta h)$ by Cd^{2+} ions

A distinct $[Cd^{2+}]$-dependent change in the viscoelastic properties of pAA-Cys5 brushes (Figure 3) strongly suggests that binding of Cd^{2+} ions modulates the interfacial potential in a $[Cd^{2+}]$-dependent manner. For this purpose, we monitored the vertical Brownian motion of latex particles (diameter of 10 μm) hovering on the surface of polymer brushes using RICM (Figure 5A). Changes in the particle height can be detected by analyzing interference patterns obtained from RICM images (Fröhlich et al., 2021). Figure 5B is an RICM snapshot of a particle hovering on the surface of pAA-Cys5 brushes at $[Cd^{2+}] =$ 0 M. The concentric rings reflect the shape of the particle. Figure 5C shows the intensity profile calculated from radial integration of the concentric interference patterns in panel b. The mean radial intensity profiles after azimuthal integration are indicated by black symbols. The radial integration was introduced to improve the accuracy for Δh determination (Fröhlich et al., 2021). Figure 5D shows the height profile of the particle calculated from the intensity profile shown in panel c using Eq. (1).

Figure 6A shows the fluctuation of the particle height recorded over time and the corresponding interfacial potential measured at $[Cd^{2+}]$ = 0 M (top), 10^{-5} M (middle), and 10^{-3} M (bottom). The plot of Δh vs. *t* clearly indicated that the amplitude

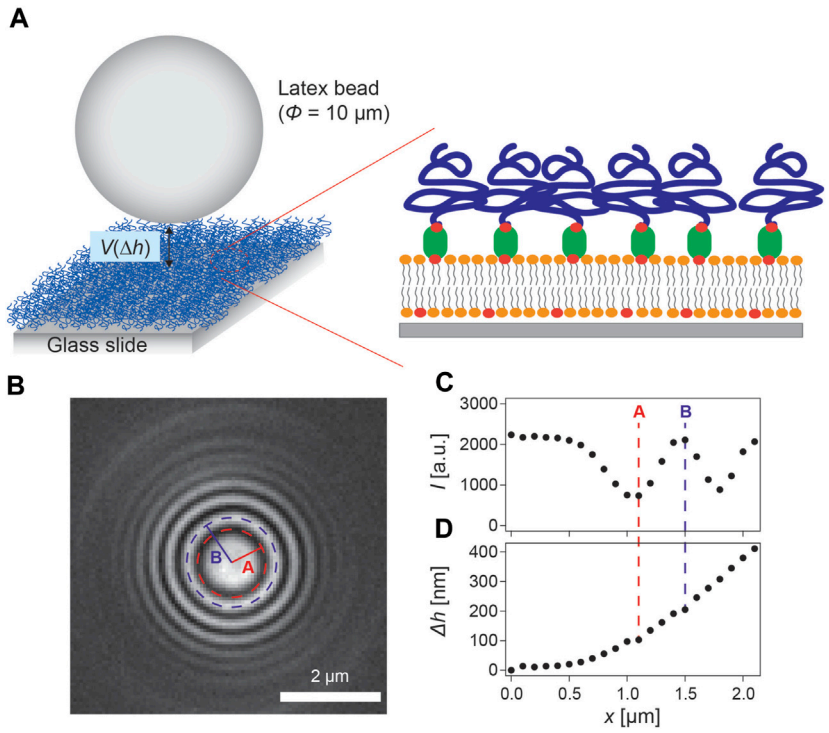

FIGURE 5
Label-free, microinterfereometric detection of a latex bead hovering on polymer brushes. **(A)** Schematic illustration of a latex particle undergoing a vertical Brownian motion on polymer brushes. **(B)** Snapshot of a latex particle on the brush surface Scale bar: 2 μm. **(C)** Intensity profile obtained by the radial integration of the concentric interference pattern in panel **(B)**. **(D)** Reconstructed relative height profile of the bead.

of height fluctuation was strongly damped at $[Cd^{2+}] = 10^{-3}$ M. The effective interfacial potential $V(\Delta h)$ calculated using Eq. 6 (Figure 6B) was well approximated by parabolic functions (solid line) described within the framework of Derjaguin's approximation for weak interactions (Derjaguin, 1987). The obtained potential curvature V'' and hence the spring constant of harmonic potential showed an increase from 0.8×10^{-21} J/nm^2 (0 M) to 5.9×10^{-21} J/nm^2 (10^{-3} M), suggesting that the particle height was sharply confined in the presence of Cd^{2+} ions. As shown in Figure 6C, the potential curvature V'' was plotted as a function of $[Cd^{2+}]$. The potential curvature V'' exhibited a clear increase at $[Cd^{2+}] \geq 10^{-4}$ M. It is notable that Δf and ΔD showed significant deviation from the swollen brushes at this concentration.

Because changes in the potential curvature may correlate with changes in hydrodynamic friction, we calculated the autocorrelation of the height fluctuation for different $[Cd^{2+}]$ (Figure 6D). The correlation functions were well fitted by single exponential functions (solid lines, Eq. 5). Increasing $[Cd^{2+}]$ led to a distinct decrease in the mean squared amplitude of fluctuation $\Delta h^2(0)$ and thus the characteristic relaxation time τ. The increase in $[Cd^{2+}]$ from 0 through 10^{-5} to 10^{-3} M resulted in a decrease in $\Delta h^2(0)$ from 5.1 through 1.9 to 0.7 nm^2, reflecting the suppression of vertical Brownian motion. As presented in Figure 6D, the relaxation time τ at $[Cd^{2+}] = 0$ M, $\tau \approx 61$ ms, showed a distinct decrease by adding $[Cd^{2+}] = 10^{-7}$ M, close to the detection limit ($\tau < 30$ ms). The data suggest that the hydrodynamic friction γ significantly increases even at the very low $[Cd^{2+}]$ not detected by the change in the potential curvature.

3.5 Effect of ion specificity on interfacial modulation

Naturally occurring proteins possessing –SH and –COOH moieties show high specificity towards heavy metal ions. Therefore, we further examined the ion specificity of pAA-Cys5 brushes by performing experiments in the presence of Ca^{2+} ions, which are similar to Cd^{2+} ions in ionic radius. Figure 7A shows the change in Δf (solid symbols) and ΔD (open symbols) of pAA-Cys0 brushes as a function of $[Ca^{2+}]$, showing distinct differences. First, the change in QCM-D response was undetectable until $[Ca^{2+}] = 10^{-4}$ M, an order of magnitude lower than the onset level for Cd^{2+}. Moreover, the change in Δf and ΔD was less pronounced compared with the response to $[Cd^{2+}]$. The differences in Δf and ΔD between

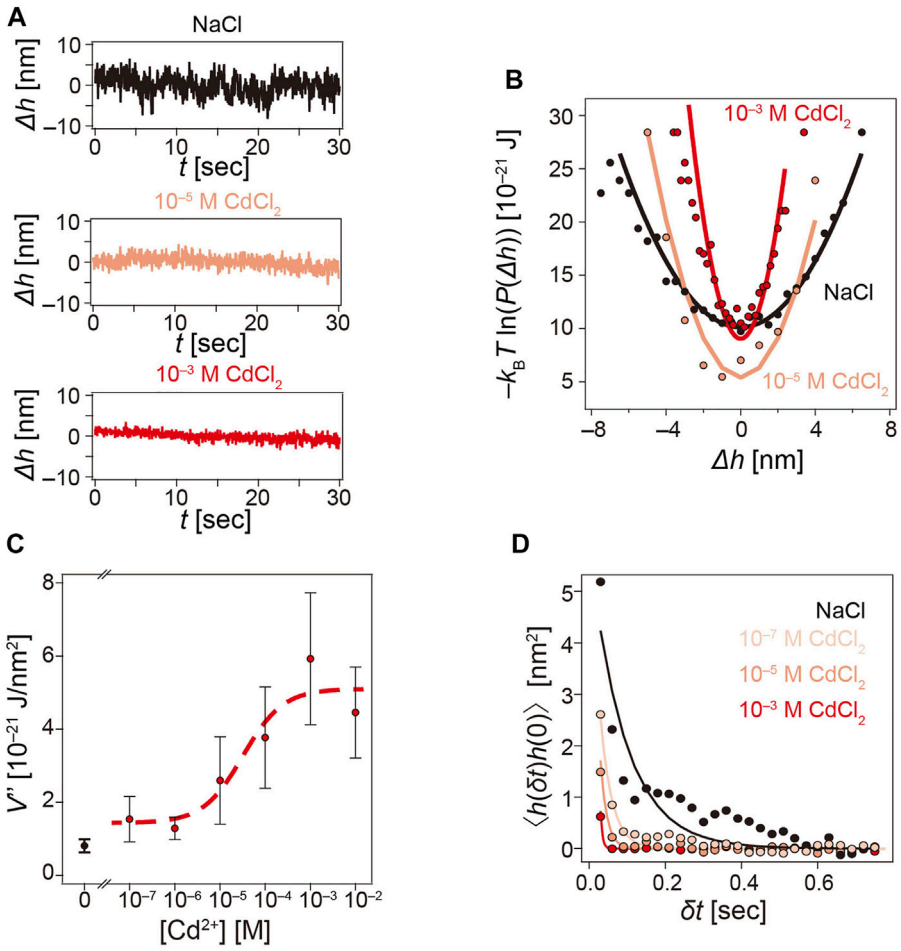

FIGURE 6
Cd^{2+}-induced modulation of interfacial potential and curvature. **(A)** Height fluctuation of latex beads monitored by RICM over time at $[Cd^{2+}]$ = 0 M, 10^{-5}, and 10^{-3} M. **(B)** Corresponding interfacial potential $V(\Delta h)$ following Eq. 6. **(C)** The potential curvature V'' plotted as a function of $[Cd^{2+}]$, exhibiting a clear increase at $[Cd^{2+}] \geq 10^{-5}$ M. **(D)** Autocorrelation function of height fluctuation calculated for $[Cd^{2+}]$ = 0, 10^{-7}, 10^{-5}, and 10^{-3} M.

$[Ca^{2+}] = 10^{-3}$ M and 0 M ($\Delta f = 5.5$ Hz and $\Delta D = -2.5 \times 10^{-6}$) were less significant compared with the response to Cd^{2+} ions (Figure 4D). The interfacial potentials $V(\Delta h)$ calculated for $[Ca^{2+}] = 10^{-6}$ and 10^{-3} M were plotted, as shown in Figure 7B. Compared with the data presented in Figure 6D, no clear differences in the global shape of the potential as well as the curvature V'' were detected, suggesting that the less pronounced change caused by Ca^{2+} binding was not enough to alter the confinement of particle position. Figures 7C, D show the response of pAA-Cys0 and pPEGMA-Cys5, respectively. The response of pAA-Cys0 to Ca^{2+} was weaker than that to Cd^{2+} (Figure 4A). The differences in Δf and ΔD between $[Ca^{2+}] = 10^{-3}$ M and 0 M were $\Delta f = -2.0$ Hz and $\Delta D = -0.3 \times 10^{-6}$, respectively. pPEGMA-Cys5 showed no detectable changes even in the presence of $[Ca^{2+}] = 10^{-3}$ M (Figure 7D). Changes in Δf and ΔD monitored over time are presented in Supplementary Figure S5. These data suggest that the response of pAA-Cys5 to Ca^{2+} is significantly enhanced by the coexistence of –SH and –COOH groups, which is similar to the data presented in Figure 4. However, the one order of magnitude lower sensitivity and very minor change in V'' observed here suggest ion-specific interaction of pAA-Cys5, that is, with Cd^{2+} ions, which may be attributed to the formation of a chelator complex, such as the one reported for *N*-acetylcysteine in aqueous solution (Jalilehvand et al., 2011).

4 Discussion

4.1 Influence of electrostatic screening

Ample studies have demonstrated that the conformation of polyelectrolyte brushes strongly depends on the pH and salt concentration (Ahrens et al., 1998; Rehfeldt et al., 2006b). So far,

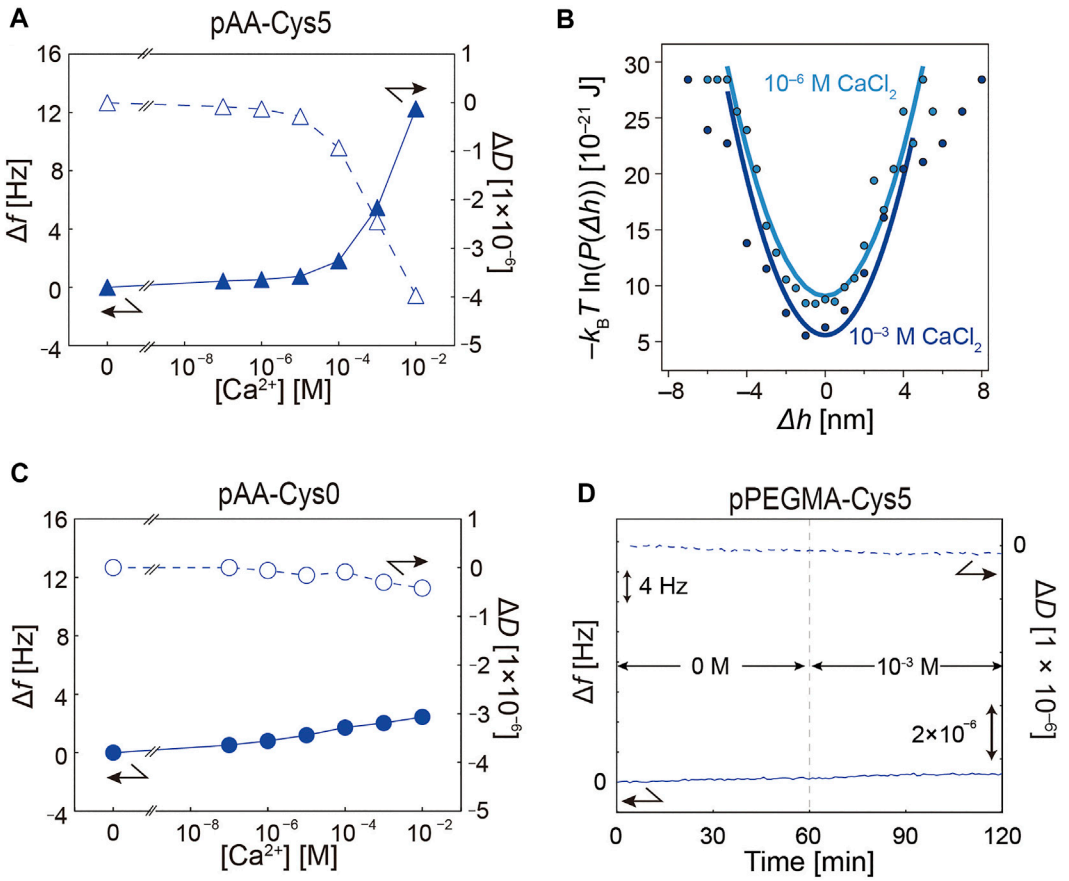

FIGURE 7
Response of polymers with different structures to $[Ca^{2+}]$. **(A)** Dependence of Δf and ΔD on $[Ca^{2+}]$ for pAA-Cys5-biotin. The response was distinctly less prominent compared to the response to $[Cd^{2+}]$ (Figure 4B). **(B)** Interfacial potentials exhibited no clear sharpening, suggesting no increase in the potential curvature V''. **(C)** pAA-Cys0 showed much weaker response to $[Ca^{2+}]$. **(D)** pPEGMA-Cys5 showed no response even at 10^{-3} M Cd^{2+}.

to highlight the influence of $[Cd^{2+}]$ and to compare the effects of Cd^{2+} and Ca^{2+} ions, we performed all experiments in the presence of 10 mM Tris-HCl and 100 mM NaCl. This enables us to sustain pH constant (7.4) and minimize crosstalk with electrostatic screening (Debye screening length $\kappa^{-1} < 1$ nm). In the next step, we removed the supporting salt (100 mM NaCl) and examined if the ion-specific response of pAA-Cys5 brushes was enhanced. Figure 8 shows the height fluctuation over time (top) and the interfacial potentials $V(\Delta h)$ (bottom) measured in 10 mM Tris-HCl (pH 7.4) in the presence of $[Na^+] = 10$ mM (a) $[Cd^{2+}] = 10$ mM (b), and $[Ca^{2+}] = 10$ mM (c). The corresponding potential curvature values were $V'' = 3.7 \times 10^{-22}$ J/nm^2 (Na^+), 125×10^{-22} J/nm^2 (Cd^{2+}), and 66×10^{-22} J/nm^2 (Ca^{2+}). It is notable that the potential curvature V'' increased by an order of magnitude by changing monovalent Na^+ ions to divalent ions, and the effect was more pronounced with Cd^{2+} ions than with Ca^{2+} ions. Distinct sharpening of the potential confinement is also a reflection of a significant increase in the hydrodynamic friction γ and hence a decrease in the relaxation time τ. As presented in Supplementary Figure S6, the relaxation time $\tau = 75$ m s could be calculated in the buffer containing NaCl, although τ was not detectable in the buffers containing $CaCl_2$ and $CdCl_2$. This seems reasonable because τ was not detectable at $[Cd^{2+}] = 10^{-6}$ M even in the presence of 100 mM NaCl.

To highlight how the presence of 100 mM NaCl affects the response of pAA-Cys5 brushes to divalent cations, we measured the zeta potential. Here, we deposited supported membranes doped with 2 mol% DOPE-biotin on porous SiO_2 microparticles (diameter 3 μm) and grafted pAA-Cys5 brushes via neutravidin crosslinkers (Figure 9A, see Supplementary Information S7 for the detail of preparation). As shown in Figure 9B, grafting of Fluor-pAA-Cys5 brushes enabled uniform coating of all particles with brushes. Figures 9C, D show the zeta potential ζ plotted as a function of $[Cd^{2+}]$ (red) and $[Ca^{2+}]$ (blue), measured in the presence and absence of 100 mM NaCl, respectively. As a general tendency, we observed a monotonic increase in ζ with

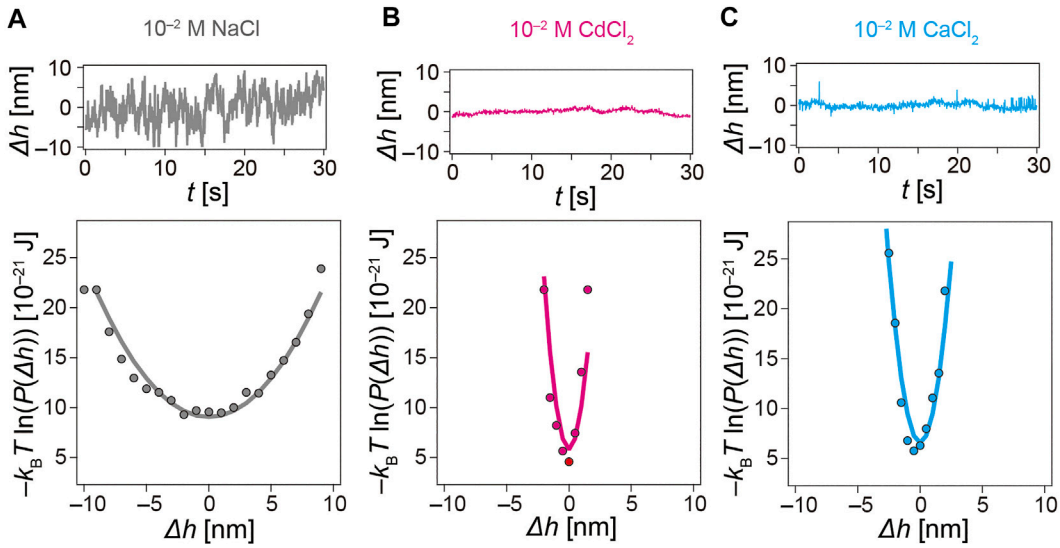

FIGURE 8
Influence of electrochemical screening on interfacial potential. Height fluctuation of latex beads monitored by RICM over time (top) and the corresponding interfacial potential (bottom). Note that the electrolytes contains only 10 mM Tris-HCl (pH 7.4) with **(A)** [NaCl] = 10^{-2} M **(B)** [$CdCl_2$] = 10^{-2} M, and **(C)** [$CaCl_2$] = 10^{-2} M.

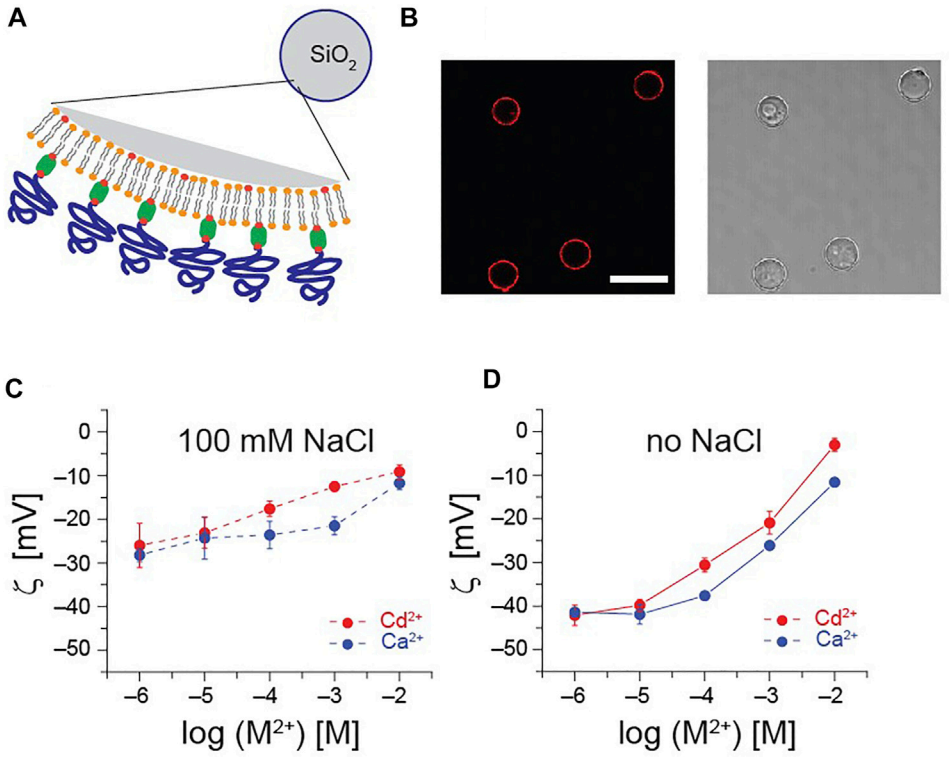

FIGURE 9
Influence of electrochemical screening on surface charges. **(A)** Schematic illustration of SiO_2 microparticle (diameter 10 μm) functionalized with pAA-Cys5 used for the zeta potential measurements. **(B)** Confocal fluorescence (left) and bright field (right) images of particles coated with brushes. Use of labeled Fluor-pAA-Cys5 brushes enables to confirm that all particles are uniformly coated with polymer brushes. Scale bar: 20 μm. Zeta potential ζ of pAA-Cys5-coated microparticles plotted measured at various [Cd^{2+}] (red) and [Ca^{2+}] blue in 10 mM Tris-HCl (pH 7.4) in the presence **(C)** and absence **(D)** of 100 mM NaCl.

increasing divalent cation concentration, and the response was more pronounced with Cd^{2+}. Remarkably, the change caused by increasing $[Cd^{2+}]$ from 10^{-6} M to 10^{-2} M showed a distinct difference: $\Delta\zeta_{100mM} \approx +15$ mV and $\Delta\zeta_{0mM} \approx +50$ mV. The stronger modulation of surface potential in the absence of supporting salt indicates that the more pronounced change in $V(\Delta h)$ presented in Figure 8 can be interpreted as the additional contribution of electrostatics.

4.2 perspectives

During the past several decades, our understanding of how polyelectrolytes interact with ions in aqueous solution has advanced significantly, from both theoretical and experimental aspects. In particular, ion-specific interactions have drawn increasing attention owing to the potential applications of polyelectrolytes in microencapsulation, controlled release, and fabrication of switchable and adaptable surfaces. Hofmeister's pioneering work on the ion-specific precipitation of proteins (Hofmeister, 1888a; Hofmeister, 1888b) was extended to explain experimental observations as a manifestation of the hydration strength, known as kosmotropes and chaotropes. However, this simple description lacks details of proteins and other biopolymers, which makes it very difficult to understand many exceptions of the Hofmeister's series (Zhang and Cremer, 2009; Jungwirth and Cremer, 2014; Gibb, 2019).

In this study, we found that the response of pAA-Cys5 brushes to Cd^{2+} was structure dependent and attributed this finding to common structural motifs, such the –SH and –COOH groups. Intriguingly, the interaction of pAA-Cys5 brushes with Ca^{2+} was approximately one order of magnitude weaker than that with Cd^{2+}, and, more remarkably, Ca^{2+} did not cause a remarkable change in the curvature of interfacial potentials. This suggests that the interaction of pAA-Cys5 with Cd^{2+} is not only stronger than but also different from that with Ca^{2+}. One possible scenario is the formation of coordination complexes with Cd^{2+}. For example, Jalilehvan et al. demonstrated that a complex formed from N-acetylcysteine and Cd^{2+} ions in aqueous solutions using NMR (Jalilehvand et al., 2011). Although these experiments with block copolymers are non-trivial owing to the presence of two different monomers, molecular-level understanding of ion-specific interactions would help us rationally design polymeric materials for the selective capture of toxic ions in our aquatic environments.

To gain molecular-scale understanding of ion-specific interactions involving biopolymers or bio-inspired polymers, another experimental challenge is to localize specific ions with high spatial resolution, that is, $\Delta r < 1$ nm. By the combination of ultrafiltration and inductively coupled plasma optical emission spectrometry (ICP-OES), it is possible to determine the amount of Cd^{2+} ions bound to 1 g of pAA-Cys5 polymer in solution (Supplementary Information S8). However, it is extremely difficult to determine how ions are associated with certain units using commonly used optical spectroscopy, such as vibrational spectroscopy. This can be overcome partially if one confines polyelectrolytes or charged biopolymers near the interface and illuminate the interface with evanescent fields, because the depth of penetration and hence the illumination volume can be modulated by adjusting the angle of incidence. Unfortunately, widely used X-ray and neutron scattering and reflectivity cannot discriminate ions, such as K^+ vs. Ca^{2+}, although these techniques detect contrast in scattering density with high spatial resolution. Previously, we reported that grazing incidence X-ray fluorescence is able to determine the density profile of specific elements/ions with an accuracy of several Å (Schneck et al., 2010; Abuillan et al., 2013). Element specific, surface sensitive techniques combined with advanced computational methods would help us not only understand the electrostatics of soft matters near the interface but also rationally design new bio-inspired materials by optimizing the molecular-level structure to gain maximum functional output.

Data availability statement

The original contributions presented in the study are included in the article/Supplementary Material further inquiries can be directed to the corresponding authors.

Author contributions

MT and MN designed and directed the research. MN and AS synthesized and characterized the polymers, and AY, KH, and SH performed the experiments and analyzed the data. MT, MN, AY, and KH wrote the manuscript, and all the authors were involved in the discussion throughout the manuscript preparation.

Funding

This study was supported by the JSPS KAKENHI (JP19H05719 to MN and MT, and JP22K18170 to KH.) and the German Science Foundation (SPP2171 Ta253/14-2 and Germany's Excellence Strategy—2082/1—390761711 to MT).

Conflict of interest

The authors declare that the research was conducted in the absence of any commercial or financial relationships that could be construed as a potential conflict of interest.

Publisher's note

Acknowledgments

AY and KH are thankful to Dr. H. Ogawa and Mr. I. Takeuchi for experimental assistance. FW thanks Dr. S. Kaufmann for helpful suggestions and Ms. A. Dudin for experimental assistance. MN and AS thank Prof. S. Sakai for insightful comments. AY thanks the Program for the Development of Next-generation Leading Scientists with Global Insight (L-INSIGHT), sponsored by the Ministry of Education, Culture, Sports, Science and Technology (MEXT), Japan. We thank Edanz (https://jp.edanz.com/ac) for editing a draft of this manuscript. MT thanks Nakatani Foundation for support.

Supplementary material

The Supplementary Material for this article can be found online at: https://www.frontiersin.org/articles/10.3389/frsfm.2022.959542/full#supplementary-material

References

Abuillan, W., Schneck, E., Körner, A., Brandenburg, K., Gutsmann, T., Gill, T., et al. (2013). Physical interactions of fish protamine and antisepsis peptide drugs with bacterial membranes revealed by combination of specular x-ray reflectivity and grazing-incidence x-ray fluorescence. *Phys. Rev. E* 88, 012705. doi:10.1103/physreve.88.012705

Ahrens, H., Förster, S., and Helm, C. A. (1998). Charged polymer brushes: Counterion incorporation and scaling relations. *Phys. Rev. Lett.* 81, 4172–4175. doi:10.1103/physrevlett.81.4172

Albersdörfer, A., and Sackmann, E. (1999). Swelling behavior and viscoelasticity of ultrathin grafted hyaluronic acid films. *Eur. Phys. J. B* 10, 663–672. doi:10.1007/s100510050898

Amadei, F., FröHlich, B., Stremmel, W., and Tanaka, M. (2018). Nonclassical interactions of phosphatidylcholine with mucin protect intestinal surfaces: A microinterferometry study. *Langmuir* 34, 14046–14057. doi:10.1021/acs.langmuir.8b03035

Arakawa, T., and Timasheff, S. N. (1984). Mechanism of protein salting in and salting out by divalent cation salts: Balance between hydration and salt binding. *Biochemistry* 23, 5912–5923. doi:10.1021/bi00320a004

Ballauff, M., and Borisov, O. (2006). Polyelectrolyte brushes. *Curr. Opin. Colloid & Interface Sci.* 11, 316–323. doi:10.1016/j.cocis.2006.12.002

Beveridge, T. (1981). Ultrastructure, chemistry, and function of the bacterial wall. *Int. Rev. Cytol.* 72, 229–317. doi:10.1016/s0074-7696(08)61198-5

Biesalski, M., Johannsmann, D., and Rühe, J. (2004). Electrolyte-induced collapse of a polyelectrolyte brush. *J. Chem. Phys.* 120, 8807–8814. doi:10.1063/1.1690242

Borisov, O. V., Zhulina, E. B., and Birshtein, T. M. (1994). Diagram of the states of a grafted polyelectrolyte layer. *Macromolecules* 27, 4795–4803. doi:10.1021/ma00095a021

Cobbett, C. S. (2000). Phytochelatin biosynthesis and function in heavy-metal detoxification. *Curr. Opin. Plant Biol.* 3, 211–216. doi:10.1016/s1369-5266(00)00066-2

Derjaguin, B. V. (1987). Some results from 50 years' research on surface forces, *Surf. Forces Surfactant Syst.*, 40. Berlin, Heidelberg: Springer, 240–251. doi:10.1016/0079-6816(92)90051-I

Förster, S., and Schmidt, M. (1995). Polyelectrolytes in solution, *Phys. Prop. Polym.*, 120. Berlin, Heidelberg: Springer Berlin Heidelberg, 51–133.

Fröhlich, B., Dasanna, A. K., Lansche, C., Czajor, J., Sanchez, C. P., Cyrklaff, M., et al. (2021). Functionalized supported membranes for quantifying adhesion of P. falciparum-infected erythrocytes. *Biophysical J.* 120, 3315–3328. doi:10.1016/j.bpj.2021.07.003

Gibb, B. C. (2019). Hofmeister's curse. *Nat. Chem.* 11, 963–965. doi:10.1038/s41557-019-0355-1

Gouin, S. (2004). Microencapsulation: Industrial appraisal of existing technologies and trends. *Trends Food Sci. Technol.* 15, 330–347. doi:10.1016/j.tifs.2003.10.005

Hamer, D. H. (1986). Metallothionein. *Annu. Rev. Biochem.* 55, 913–951. doi:10.1146/annurev.bi.55.070186.004405

Herrmann, M., Schneck, E., Gutsmann, T., Brandenburg, K., and Tanaka, M. (2015). Bacterial lipopolysaccharides form physically cross-linked, two-dimensional gels in the presence of divalent cations. *Soft Matter* 11, 6037–6044. doi:10.1039/c5sm01002k

Higaki, Y., Fröhlich, B., Yamamoto, A., Murakami, R., Kaneko, M., Takahara, A., et al. (2017). Ion-specific modulation of interfacial interaction potentials between solid substrates and cell-sized particles mediated via zwitterionic, super-hydrophilic poly(sulfobetaine) brushes. *J. Phys. Chem. B* 121, 1396–1404. doi:10.1021/acs.jpcb.6b11540

Hofmeister, F. (1888a). Zur Lehre von der Wirkung der Salze. *Arch. f. Exp. Pathol. u. Pharmakol.* 25, 1–30. doi:10.1007/bf01838161

Hofmeister, F. (1888b). Zur lehre von der wirkung der salze: Zweite mittheilung. *Arch. f. Exp. Pathol. u. Pharmakol.* 24, 247–260. doi:10.1007/bf01918191

Hollingsworth, N. R., Wilkanowicz, S. I., and Larson, R. G. (2019). Salt- and pH-induced swelling of a poly(acrylic acid) brush via quartz crystal microbalance w/dissipation (QCM-D). *Soft Matter* 15, 7838–7851. doi:10.1039/c9sm01289c

Israelachvili, J. N. (1985). *Intermolecular and surface forces with applications to colloidal and biological systems*. Amsterdam, Netherlands: Elsevier.

Jalilehvand, F., Amini, Z., Parmar, K., and Kang, E. Y. (2011). Cadmium (II) N-acetylcysteine complex formation in aqueous solution. *Dalton Trans.* 40, 12771. doi:10.1039/c1dt11705j

Jungwirth, P., and Cremer, P. S. (2014). Beyond hofmeister. *Nat. Chem.* 6, 261–263. doi:10.1038/nchem.1899

Kaindl, T., Rieger, H., Kaschel, L.-M., Engel, U., Schmaus, A., Sleeman, J., et al. (2012). Spatio-temporal patterns of pancreatic cancer cells expressing CD44 isoforms on supported membranes displaying hyaluronic acid oligomers arrays. *PLOS ONE* 7, e42991. doi:10.1371/journal.pone.0042991

Keller, C. A., Glasmästar, K., Zhdanov, V. P., and Kasemo, B. (2000). formation of supported membranes from vesicles. *Phys. Rev. Lett.* 84, 5443–5446. doi:10.1103/physrevlett.84.5443

Kern, W., and Puotinen, D. A. (1970). Cleaning solutions based on hydrogen peroxide for use in silicon semiconductor technology. *RCA Rev.* 31, 187–206. doi:10.1029/RS005i012p01489

Körner, A., Deichmann, C., Rossetti, F. F., Köhler, A., Konovalov, O. V., Wedlich, D., et al. (2013). Cell differentiation of pluripotent tissue sheets immobilized on supported membranes displaying cadherin-11. *PLOS ONE* 8, e54749. doi:10.1371/journal.pone.0054749

Langmuir, I., and Schaefer, V. J. (1938). Activities of urease and pepsin monolayers. *J. Am. Chem. Soc.* 60, 1351–1360. doi:10.1021/ja01273a023

Makky, A., and Tanaka, M. (2015). Impact of lipid oxidization on biophysical properties of model cell membranes. *J. Phys. Chem. B* 119, 5857–5863. doi:10.1021/jp512339m

Mehringer, J., Hofmann, E., Touraud, D., Koltzenburg, S., Kellermeier, M., Kunz, W., et al. (2021). Salting-in and salting-out effects of short amphiphilic molecules: A

balance between specific ion effects and hydrophobicity. *Phys. Chem. Chem. Phys.* 23, 1381–1391. doi:10.1039/d0cp05491g

Miller, S., Dykes, D., and Polesky, H. (1988). A simple salting out procedure for extracting DNA from human nucleated cells. *Nucleic Acids Res.* 16, 1215. doi:10.1093/nar/16.3.1215

Monzel, C., Veschgini, M., Madsen, J., Lewis, A. L., Armes, S. P., Tanaka, M., et al. (2015). Fine adjustment of interfacial potential between pH-responsive hydrogels and cell-sized particles. *Langmuir* 31, 8689–8696. doi:10.1021/acs.langmuir.5b01896

Morris, E. R., Rees, D. A., Thom, D., and Boyd, J. (1978). Chiroptical and stoichiometric evidence of a specific, primary dimerisation process in alginate gelation. *Carbohydr. Res.* 66, 145–154. doi:10.1016/s0008-6215(00)83247-4

Moya, S., Azzaroni, O., Farhan, T., Osborne, V. L., and Huck, W. T. S. (2005). Locking and unlocking of polyelectrolyte brushes: Toward the fabrication of chemically controlled nanoactuators. *Angew. Chem. Int. Ed.* 44, 4578–4581. doi:10.1002/anie.200500228

Oliveira, R. G., Schneck, E., Quinn, B. E., Konovalov, O. V., Brandenburg, K., Seydel, U., et al. (2009). Physical mechanisms of bacterial survival revealed by combined grazing-incidence X-ray scattering and Monte Carlo simulation. *Comptes Rendus Chim.* 12, 209–217. doi:10.1016/j.crci.2008.06.020

Pincus, P. (1991). Colloid stabilization with grafted polyelectrolytes. *Macromolecules* 24, 2912–2919. doi:10.1021/ma00010a043

Pink, D. A., Truelstrup Hansen, L., Gill, T. A., Quinn, B. E., Jericho, M. H., Beveridge, T. J., et al. (2003). Divalent calcium ions inhibit the penetration of protamine through the polysaccharide brush of the outer membrane of gram-negative bacteria. *Langmuir* 19, 8852–8858. doi:10.1021/la030193e

Rehfeldt, F., Steitz, R., Armes, S. P., von Klitzing, R., Gast, A. P., Tanaka, M., et al. (2006a). Reversible activation of diblock copolymer monolayers at the interface by pH modulation, 1: Lateral chain density and conformation. *J. Phys. Chem. B* 110, 9171–9176. doi:10.1021/jp054532j

Rehfeldt, F., Steitz, R., Armes, S. P., von Klitzing, R., Gast, A. P., Tanaka, M., et al. (2006b). Reversible activation of diblock copolymer monolayers at the interface by pH modulation, 2: Membrane interactions at the solid/liquid interface. *J. Phys. Chem. B* 110, 9177–9182. doi:10.1021/jp054533b

Reynolds, O. (1883). XXIX. An experimental investigation of the circumstances which determine whether the motion of water shall be direct or sinuous, and of the law of resistance in parallel channels. *Philosophical Trans. R. Soc. Lond.* 174, 935–982. doi:10.1098/rstl.1883.0029

Rieger, H., Yoshikawa, H. Y., Quadt, K., Nielsen, M. A., Sanchez, C. P., Salanti, A., et al. (2015). Cytoadhesion of Plasmodium falciparum–infected erythrocytes to chondroitin-4-sulfate is cooperative and shear enhanced. *Blood* 125, 383–391. doi:10.1182/blood-2014-03-561019

Rühe, J., Ballauff, M., Biesalski, M., Dziezok, P., Gröhn, F., Johannsmann, D., et al. (2004). "Polyelectrolyte brushes," in *Polyelectrolytes with defined molecular architecture I*. Editor M. Schmidt (Berlin, Heidelberg: Springer Berlin Heidelberg).

Schneck, E., Papp-Szabo, E., Quinn, B. E., Konovalov, O. V., Beveridge, T. J., Pink, D. A., et al. (2009). Calcium ions induce collapse of charged O-side chains of lipopolysaccharides from *Pseudomonas aeruginosa*. *J. R. Soc. Interface* 6, S671–S678. doi:10.1098/rsif.2009.0190.focus

Schneck, E., Schubert, T., Konovalov, O. V., Quinn, B. E., Gutsmann, T., Brandenburg, K., et al. (2010). Quantitative determination of ion distributions in bacterial lipopolysaccharide membranes by grazing-incidence X-ray fluorescence. *Proc. Natl. Acad. Sci. U. S. A.* 107, 9147–9151. doi:10.1073/pnas.0913737107

Seyrek, E., Dubin, P. L., Tribet, C., and Gamble, E. A. (2003). Ionic strength dependence of protein-polyelectrolyte interactions. *Biomacromolecules* 4, 273–282. doi:10.1021/bm025664a

Shindo, H., and Brown, T. L. (1965). Infrared spectra of complexes of L-cysteine and related compounds with zinc(II), cadmium(II), mercury(II), and lead(II)[1]. *J. Am. Chem. Soc.* 87, 1904–1909. doi:10.1021/ja01087a013

Stuart, M. A. C., Huck, W. T. S., Genzer, J., Müller, M., Ober, C., Stamm, M., et al. (2010). Emerging applications of stimuli-responsive polymer materials. *Nat. Mat.* 9, 101–113. doi:10.1038/nmat2614

Thiele, H. F. (1967). *Histolyse und Histogenese: Gewebe und ionotrope Gele; Prinzip einer Strukturbildung*. Frankfurt, Akad: Verl.-Ges.

Tomé, L. I. N., Pinho, S. P., Jorge, M., Gomes, J. R. B., and Coutinho, J. A. P. (2013). Salting-in with a salting-out agent: Explaining the cation specific effects on the aqueous solubility of amino acids. *J. Phys. Chem. B* 117, 6116–6128. doi:10.1021/jp4021307

Vogt, B. D., Lin, E. K., Wu, W.-L., and White, C. C. (2004). Effect of film thickness on the validity of the sauerbrey equation for hydrated polyelectrolyte films. *J. Phys. Chem. B* 108, 12685–12690. doi:10.1021/jp0481005

Wu, T., Gong, P., Szleifer, I., Vlček, P., Šubr, V., Genzer, J., et al. (2007). Behavior of surface-anchored poly(acrylic acid) brushes with grafting density gradients on solid substrates: 1. Experiment. *Macromolecules* 40, 8756–8764. doi:10.1021/ma0710176

Zhang, Y., and Cremer, P. S. (2009). The inverse and direct Hofmeister series for lysozyme. *Proc. Natl. Acad. Sci. U. S. A.* 106, 15249–15253. doi:10.1073/pnas.0907616106

Zhou, F., and Huck, W. T. S. (2006). Surface grafted polymer brushes as ideal building blocks for "smart" surfaces. *Phys. Chem. Chem. Phys.* 8, 3815–3823. doi:10.1039/b606415a

Zhulina, E. B., Birshtein, T. M., and Borisov, O. V. (1995). Theory of ionizable polymer brushes. *Macromolecules* 28, 1491–1499. doi:10.1021/ma00109a021